Au@pNIPAM Thermosensitive Nanostructures: Control over Shell Cross-linking, Overall Dimensions, and Core Growth

ARTICLE *in* ADVANCED FUNCTIONAL MATERIALS · OCTOBER 2009

Impact Factor: 11.81 · DOI: 10.1002/adfm.200900481

6 AUTHORS, INCLUDING:

Rafael Contreras
University of Malaga
22 PUBLICATIONS **470** CITATIONS
SEE PROFILE

Isabel Pastoriza-Santos
University of Vigo
146 PUBLICATIONS **9,133** CITATIONS
SEE PROFILE

Jorge Pérez-Juste
University of Vigo
214 PUBLICATIONS **7,754** CITATIONS
SEE PROFILE

Antonio Fernández-Barbero
Universidad de Almería
97 PUBLICATIONS **1,762** CITATIONS
SEE PROFILE

FULL PAPER

Au@pNIPAM Thermosensitive Nanostructures: Control over Shell Cross-linking, Overall Dimensions, and Core Growth

By *Rafael Contreras-Cáceres, Jessica Pacifico, Isabel Pastoriza-Santos, Jorge Pérez-Juste,* Antonio Fernández-Barbero,* and *Luis M. Liz-Marzán*

Thermoresponsive nanocomposites comprising a gold nanoparticle core and a poly(*N*-isopropylacrylamide) (pNIPAM) shell are synthesized by grafting the gold nanoparticle surface with polystyrene, which allows the coating of an inorganic core with an organic shell. Through careful control of the experimental conditions, the pNIPAM shell cross-linking density can be varied, and in turn its porosity and stiffness, as well as shell thickness from a few to a few hundred nanometers is tuned. The characterization of these core–shell systems is carried out by photon-correlation spectroscopy, transmission electron microscopy, and atomic force microscopy. Additionally, the porous pNIPAM shells are found to modulate the catalytic activity, which is demonstrated through the seeded growth of gold cores, either retaining the initial spherical shape or developing a branched morphology. The nanocomposites also present thermally modulated optical properties because of temperature-induced local changes of the refractive index surrounding the gold cores.

1. Introduction

The synthesis of core–shell nanocomposites, with a shell of either an inorganic or organic material coating an inorganic nanoparticle core has been thoroughly investigated during the last decades.[1,2] The main goals so far have been to improve the colloidal stability of the particles or obtaining new properties from the combination of materials within the heterostructure. For instance, silica-coated metal,[3] magnetic,[4] and semiconductor nanoparticles[5] are good examples of inorganic–inorganic core–shell systems. In these cases, the silica shells confer a greater stability to the particles and facilitate the subsequent functionalization by means of silane chemistry.[6] Whereas inorganic shells are usually grown from the nanoparticle core surface, organic shells can be deposited on inorganic cores in different ways, such as nanoparticle synthesis in the presence of a polymeric ligand,[7,8] attachment of functionalized polymers to the surface,[9] layer-by-layer deposition,[10,11] and polymerization from particle-bound initiators.[12,13] These possibilities usually require a specific chemical interaction between the particle's surface and the polymer. The nature of the organic polymeric shell can vary from amine or thiol-terminated linear polymers[8,14,15] or block-copolymers[16–18] to cross-linked polymers.[19,20] Among the different polymer shells, stimuli-responsive materials are particularly interesting because of the additional possibility of manipulation through external stimuli.[19,21,22] We have recently proposed a method for coating gold nanoparticles with thermoresponsive polymer shells, which have been shown to allow modulation of the optical properties of these systems, as well as enhancing the opportunities to use the gold cores as surface-enhanced Raman scattering (SERS) supports, exploiting shell porosity and temperature-dependent solubility.[19,23]

The procedure for coating the nanoparticles with the polymer (microgel) shell involves two different steps, with the first step comprising the growth of a thin polystyrene layer, followed by polymerization of *N*-isopropylacrylamide (NIPAM) on the polystyrene-coated nanoparticles. As envisaged in our previous work,[19] the initial coating of the nanoparticles requires the presence of a cationic surfactant (cetyltrimethylammonium bromide, CTAB), which readily adsorbs onto gold surfaces through the bromide ions (see Scheme 1) and forms a bilayer, which is crucial to stabilizing the particles. This CTAB bilayer provides a relatively thick (ca. 3nm) hydrophobic environment, which can sequester hydrophobic organic molecules from the aqueous solution.[24] Therefore, water-insoluble styrene and divinylbenzene (DVB) are expected to be distributed mainly within both the CTAB micelles and the CTAB bilayer on the gold surfaces. Upon equilibration, the addition of a suitable initiator leads to the polymerization of styrene (to polystyrene, PS) and divinylbenzene around the gold nanoparticles but maintaining

[*] R. Contreras-Cáceres, Dr. J. Pacifico, Dr. I. Pastoriza-Santos, Dr. J. Pérez-Juste, Prof. L. M. Liz-Marzán
Departamento de Química Física and
Unidad Asociada CSIC-Universidade de Vigo
36310 Vigo (Spain)
E-mail: juste@uvigo.es
R. Contreras-Cáceres, Prof. A. Fernández-Barbero
Departamento de Física Aplicada
Universidad de Almería
Almería (Spain)

DOI: 10.1002/adfm.200900481

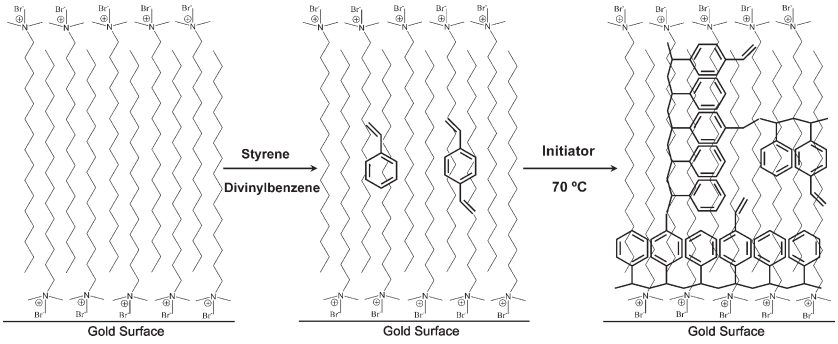

Scheme 1. Cartoon illustrating, from left to right, the CTAB bilayer formation on a gold surface, the distribution of styrene and divinylbenzene, and their polymerization.

non-polymerized vinyl groups available at the surface (see Scheme 1). The presence of vinyl groups on the surface of the gold nanoparticles has been proven by Raman spectroscopy. Figure S1, in the Supporting information, shows the Raman spectra of the PS/DVB coated particles together with a polystyrene standard. The coated particles present a band at 1630 cm^{-1} ascribed to the stretching vibration of the aliphatic vinyl group. Once the gold nanoparticles have been coated with the thin polystyrene shell, they are suitable to act as seeds for NIPAM polymerization through a standard surfactant-free polymerization process.[25] Additionally, a control experiment was performed where the NIPAM/BIS (bisacrylamide) polymerization was carried out in the presence of CTAB-stabilized nanoparticles (0.9 mM CTAB), giving rise to the formation of small microgel particles of around 60 nm and non-coated gold nanoparticles (see Figure S2 in the Supporting Information). Therefore, the initial PS/DVB coating is needed to achieve the successful encapsulation of the nanoparticles.

In this work we describe the versatile synthesis of Au@pNIPAM core–shell colloids with full control over the cross-linking density of the pNIPAM shell as well as its dimensions. The high porosity of the pNIPAM shells allowed us to control the growth of the gold cores, either retaining the initial spherical shape or developing a branched (flower/star-like) morphology based on the control of the gold salt reduction rate.

2. Results and Discussion

2.1. Influence of Cross-Linker Concentration

The range of properties and applications of Au@pNIPAM core–shell particles can be largely enhanced if we can control the cross-linking density and the thickness of the pNIPAM shell. The variation of the cross-linking degree in the pNIPAM shells has been investigated by gradually increasing the percentage of BIS in the mixture prior to polymerization, while keeping the amount of NIPAM monomers constant. The BIS content was varied between 5% and 17.5%, since higher percentages were found to lead to non-homogeneous coating of the gold particles. Figure 1 shows representative transmission electron microscopy (TEM) images of Au@pNIPAM composites with different BIS concentrations, which seem to indicate that higher cross-linker contents lead to thinner microgel shells. The thermoresponsive properties of these core–shell systems were initially characterized by photon-correlation spectroscopy (PCS). Figure 1D displays the variation of the hydrodynamic diameter of the different nanocomposites when the temperature was varied between 5 and 55 °C. In all cases, a well-defined volume phase-transition temperature around 35 °C was determined, with a slope that increased as the cross-linker content was decreased. At high temperatures, when the pNIPAM shell is completely collapsed, the measured mean diameter of the different core–shell systems was similar in all cases (ca. 210 nm, that is, a gold core of 59 nm diameter and a collapsed pNIPAM shell thickness around 75 nm), whereas at low temperatures (swollen microgel), the total particle size markedly varied as a function of the degree of cross-linking. As expected, when a lower amount of BIS was used, bigger particles were formed, because of the lower degree of cross-linking of the pNIPAM chains.[25] This effect can be easily visualized if we plot the shrinking ratio versus temperature for the different nanocomposites (see Fig. 1D). The shrinking ratio (the inverse of the swelling ratio) is defined as the ratio between the volume of the particle in the fully swollen state (at 15 °C) and the volume of the particle at each temperature ($\beta = V_{swollen}(15\,°C)/V(T)$). For this particular case a 3.5× decrease in the BIS content (from 17.5% down to 5%) produces an increase of the volume in the swollen state of around 1.7 times. This effect is also evidenced in the TEM images (Fig. 1A–C), where the samples with a lower cross-linking density display a more spread

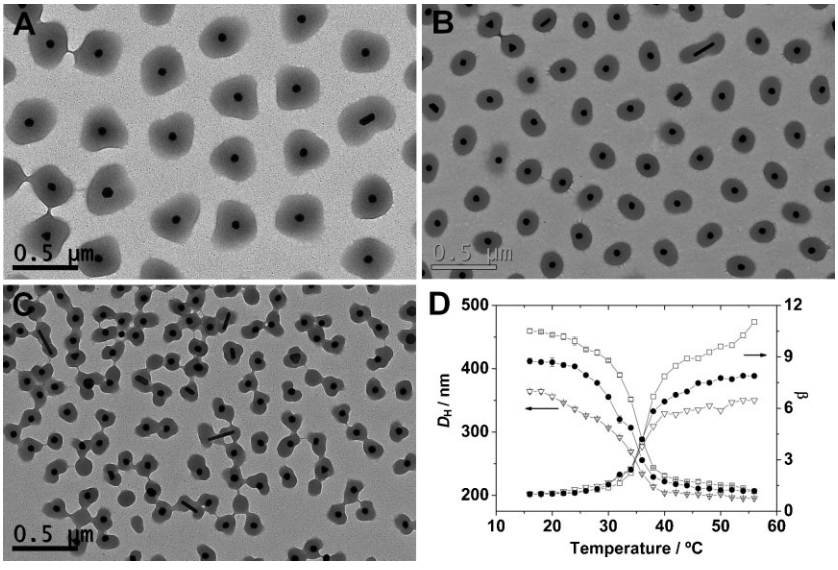

Figure 1. A–C) Representative TEM images of Au@pNIPAM core–shell particles with different BIS percentages: A) 5%, B) 10%, and C) 17.5%. D) Temperature dependence of the hydrodynamic diameter and the shrinking ratio for the different systems; (□) 5%, (•) 10%, and (▽) 17.5% BIS.

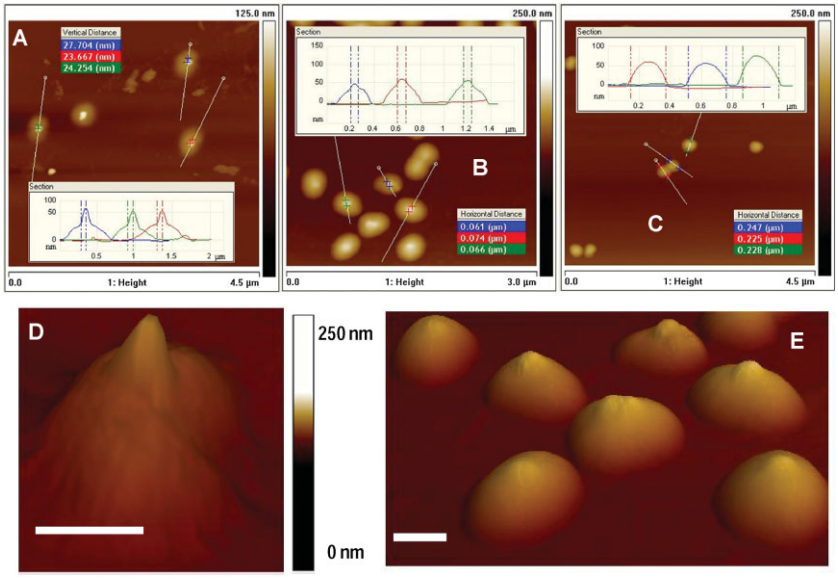

Figure 2. A–C) 4.5 μm × 4.5 μm (A and C) and 3.0 μm × 3.0 μm, B) AFM topography images of Au@NIPAM particles with 5% (A), 10% (B), and 17.5% (C) cross-linker. D,E) 3D plots of Au@pNIPAM composite particles with 5% and 10% cross-linker, respectively. Scale bars represent 100 nm.

pNIPAM shell, as compared to the more densely cross-linked ones.

Additional evidence of the influence of the cross-linker content on the morphology of the particles and (in particular) the rigidity of the pNIPAM shell was obtained from atomic force microscopy (AFM). The AFM measurements were performed in the tapping mode on dry core–shell microgel samples, providing confirmation of a core–shell structure, because the pNIPAM shells are spread on the gold cores when dehydrated. Figure 2A–C shows the AFM topography images for samples with 5%, 10%, and 17.5% BIS. The height profiles (insets in Fig. 2) clearly show that the core gold particles protrude out from the polymer shell at lower cross-linker percentages (5% and 10%) while for the highest BIS content (17.5%) protrusions are not seen because of the higher rigidity of the shell. Clear differences can also be observed in the 3D images (Fig. 2D,E) between the samples with 5% and 10% BIS. It should be pointed out that the cross-linking density is also reflected in the ''dry'' particle size, since less cross-linked pNIPAM shells can spread further during drying.

2.2. Controlling pNIPAM Shell Thickness

Another important factor in the design of this new class of nanocomposites is the control over the thickness of the pNIPAM polymer shell, since it can be used to modulate the properties of the gold core. The difficulty in preparing small microgel particles by surfactant-free methods has been related to an insufficient available charge to stabilize high concentrations of small particles.[25] This can in principle be overcome by two different approaches, namely either by decreasing the amount of NIPAM monomer or by adding small amounts (below the critical micelle concentration, cmc) of sodium dodecyl sulfate (SDS),[26] using 10% BIS in both cases.

Before we continue with this discussion, it should be pointed out that the growth of pNIPAM shells on the metal cores is always accompanied by a relatively high amount of free pNIPAM microgel spheres (as a result of pNIPAM nucleation). Generally, up to 70% are free pNIPAM microgels which can be easily removed through a few centrifugation/redispersion cycles because of the extremely high difference in density between the Au@pNIPAM nanocomposites and free microgels (see Experimental section). Therefore, proper control over the nucleation and growth of pNIPAM is required to tune the pNIPAM shell thickness and it can be achieved by varying the amount of either NIPAM or SDS. A decrease in monomer concentration would lead to smaller microgels (and also thinner pNIPAM shells), with a relatively small influence on secondary nucleation, while increasing the SDS concentration at a constant amount of NIPAM would favor nucleation, thereby forming smaller microgels (and thinner shells).

The results for varying the NIPAM concentration are summarized in Figure 3. Figure 3A shows the temperature dependence of the hydrodynamic diameter of core–shell colloids prepared with total amounts of the NIPAM/BIS mixture that were 75%, 50%, and 40% of the standard amount (as defined in the Experimental Section and Table S1, Supporting Information). It can be clearly seen that, as the amount of monomer is decreased, the hydrodynamic diameters of both the swollen and collapsed states decrease accordingly, in agreement with the corresponding TEM images (Fig. 3B–D). Interestingly, as the amount of NIPAM is decreased, the lower critical solution temperature is shifted toward higher values. While the sample with 75% monomer still presents a similar lower critical solution temperature (LCST) to pure pNIPAM (35 °C), in the core–shell systems with 50% and 40% monomer the LCST is shifted to higher temperatures, namely to 39 °C and 41 °C, respectively. Control experiments were carried out to analyze the polymerization of different amounts of pure NIPAM in the absence of gold nanoparticles (see Fig. S3, Supporting Information), which confirmed that a decrease in the amount of NIPAM results in decreased particle size, as well as a shift of the LCST toward higher temperatures. The LCST shift to higher temperatures could be explained by the charge density on the surface of the particles. A lower amount of monomer mixture at constant initiator concentration leads to a higher charge density, which increases the electrostatic component that tends to swell the microgel. This component competes directly against temperature, which promotes microgel shrinking.[27] Hence, a higher temperature is necessary to reach the same shrinking ratio. The variable cross-linking concentration is not responsible for this effect since it has been shown that a 40-fold change in the cross-linking concentration in pure microgels does not modify the LCST (see previous work[28]).

The second approach to control the thickness of the pNIPAM shell was based on the control of secondary nucleation, through the addition of SDS. As indicated above, the preparation of small

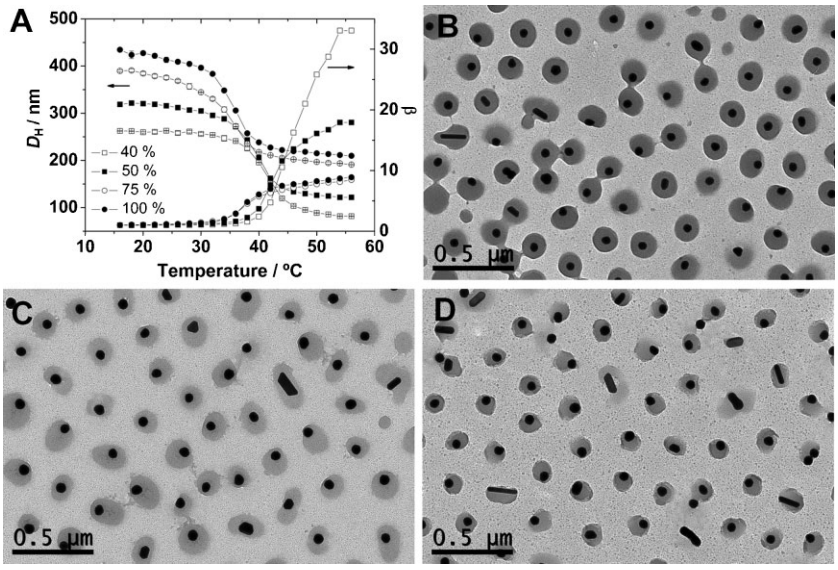

Figure 3. A) Temperature dependence of the hydrodynamic diameter and shrinking ratio for different amounts of NIPAM (percentages referred to the standard amount), as indicated in the labels. B–D) Representative TEM images of Au@pNIPAM core–shell particles obtained with different NIPAM amounts: 75% (B), 50% (C), and 40% (D).

microgels by surfactant-free methods is difficult because of the limited availability of charge to stabilize high concentrations of small particles. McPhee et al. have shown that the addition of small amounts of SDS, with concentrations below the cmc, somehow increases the rate of polymerization, leading to nanometer-size pNIPAM microgels.[26] Figure S4 (Supporting Information) shows the temperature variation of the hydrodynamic diameter, as well as representative TEM images for different core–shell systems synthesized in the presence of small amounts of SDS. It can clearly be observed that the presence of surfactant (2.5 mM and 3.5 mM) leads to a decrease in the particle size in the swollen/collapsed state from 427/230 nm (in the absence of surfactant) to 310/154 nm and 223/114 nm, respectively, thus confirming the validity of this approach. This decrease in the pNIPAM shell thickness is a consequence of a higher nucleation leading to an increase in the percentage of free pNIPAM microgels (ca. 85%), that can be easily removed from the Au@pNIPAM nanocomposites through centrifugation/redispersion cycles because of the large density difference.

Comparison of the temperature-dependent particle-size profiles obtained from PCS measurements for Au@pNIPAM composites fabricated through both described approaches (see Figs. 3A and S4D, Supporting Information) evidences a different thermoresponsive behavior of the pNIPAM shells. Whereas the decrease of the total amount of NIPAM/BIS monomers produces a shift of the LCST toward higher temperatures, the presence of SDS leads to smaller microgel shells but the LCST remains constant and similar to that of pure pNIPAM microgels (35 °C). This different thermoresponsive behavior is likely related to the difference in heterogeneity resulting from the polymerization processes. However, further studies need to be carried out to understand the observed LCST shift derived from a decrease in the amount of NIPAM monomers.

2.3. In Situ Modulation of the Au Core Morphology

We have recently demonstrated that the particle size and shape of the gold cores in Au@pNIPAM colloids can be modulated through careful control of the experimental conditions during in-situ seeded growth,[29] through the reduction of $HAuCl_4$ by ascorbic acid in the presence of CTAB.[19] It has been reported that the complexation of tetrachloroauric acid with CTAB molecules leads to a change in the redox potential of Au^{III}, in such a way that the addition of ascorbic acid can only reduce Au^{III} to Au^{I} and not to Au^{0}.[30] However, addition of gold seeds favors the catalytic reduction of the gold salt complex by this mild reducing agent, so that it takes place selectively at the metal surface. It should be pointed out that the initial polystyrene coating is believed to be far from being completely homogeneous, so that the gold salt precursor should be able to reach the gold nanoparticle surface easily.

In this process, particle-shape control can be achieved by simply changing the concentration of CTAB in the growth solution. While high CTAB concentrations (100 mM) lead to uniform growth retaining the spherical shape, lower CTAB concentrations (8 mM) result in branched nanoparticles because of a non-homogenous growth of the initially spherical nanoparticles. Figure 4 shows representative TEM images together with the UV-vis spectra of the corresponding aqueous colloids. The changes in the final particle shape are likely to arise from the different growth kinetics during gold reduction, for varying CTAB concentrations. We thus carried out a kinetic study keeping constant the amount of gold salt, gold seeds, and ascorbic acid but changing the CTAB concentration (see Experimental Section for details). Figure 4A (inset) displays the kinetic traces from the absorbance at 400 nm for both 8 mM and 0.1 M CTAB, showing that with 8mM CTAB the gold salt reduction is twice faster than with 0.1 M CTAB. This result is clearly in favor of a fully kinetic growth control; that is to say that in the presence of high CTAB concentrations the low reduction rate of the gold salt leads to a more homogenous particle growth, whereas the faster rate at low CTAB concentrations results in non-homogeneous growth. Apart from the kinetic trace, it is also interesting to see the actual evolution of the spectral features for the two different concentrations. At high concentration, the spectra invariably display a single surface-plasmon band (SPB) with increasing intensity while gradually red-shifting from 537 nm (for the starting 5 nm gold spheres) to 585 nm, corresponding to the 120 nm final spheres. On the contrary, for low CTAB concentration a new band around 600 nm appears at the early stages of the reaction which gradually red-shifts up to 792 nm, while a less intense band remains around 536 nm. These two bands are attributed to dipolar resonances, localized at either the tips or the central core of the particles, as previously shown for gold nanostars.[31]

Therefore, the final shape of the gold cores is governed by a balance between the CTAB concentration and the Au reduction

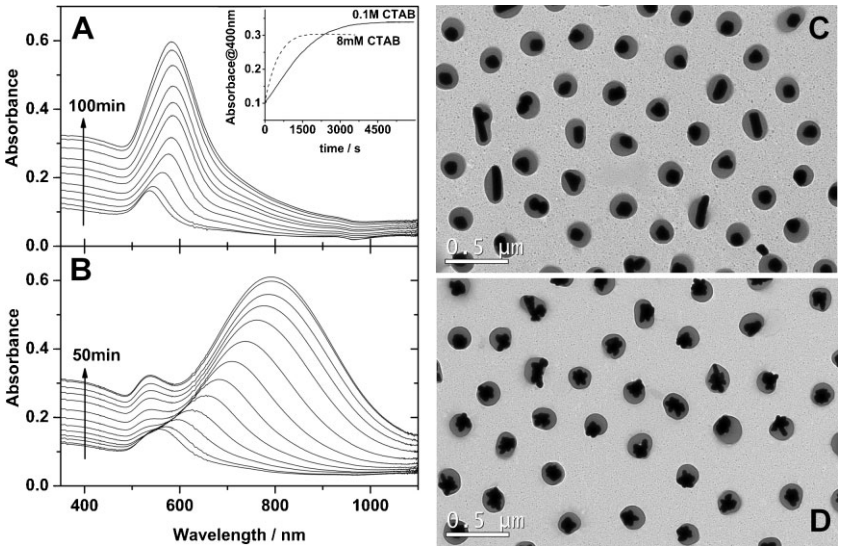

Figure 4. A,B) UV–Vis spectral evolution during the overgrowth of Au@pNIPAM (10% BIS, ratio AA/$HAuCl_4$ 16:1) in the presence of 0.1 M CTAB (A) and 8 mM CTAB (B). The inset in A shows the kinetic traces at 400 nm. C,D) TEM images of the Au@pNIPAM particles grown in 0.1 M CTAB (C) and 8 mM CTAB (D).

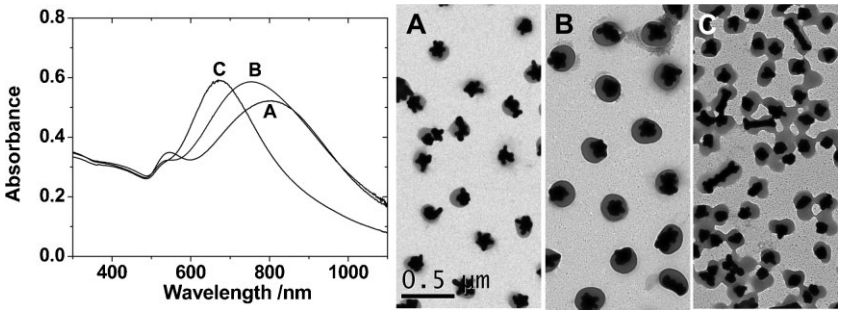

Figure 5. UV–Vis spectra and the corresponding TEM images of the overgrown Au@pNIPAM nanocomposites in the presence of 8 mM CTAB, ascorbic acid/$HAuCl_4$ ratio of 16:1 and different cross-linking densities; A) 5%, B) 10%, and C) 17.5%.

rate. This can be additionally demonstrated by affecting the reduction rate through varying the ascorbic acid (AA) concentration, at both selected CTAB concentrations. Whereas at 0.1 M CTAB concentration spherical particles were obtained regardless of the AA/Au^{III} ratio (see Fig. S5, Supporting Information), at 8 mM CTAB an increase in the AA concentration from 0.5 mM (AA/Au^{III} ratio = 4) to 2 mM (AA/Au^{III} ratio = 16) gave rise to a surface-plasmon red-shift from 667 nm to 782 nm (see Fig. S6, Supporting Information). This shift is not necessarily due to an increasing number of tips in the particles but to morphological changes such as tip aperture angle or surface roughness.[31] AFM characterization of these nanocomposites with highly branched cores (Fig. S7, Supporting Information) shows rough particles because various tips stand out from the microgel shell. The AFM height image shows such features, which are confirmed in the phase image.

So far, we have repeatedly demonstrated that if we play around with reactant concentrations, the core morphology can be tuned and all the results seem to point toward a kinetic control of the nanoparticles growth. In the core–shell system that we are using, kinetics is not only governed by the actual reaction rate at the core surface, but also by the diffusion rate of the reactants through the porous shells toward the cores. Since diffusion of the Au^{III}-CTA complex through the polymer shell can be affected by the pNIPAM microgel porosity, we expected that changing the percentage of cross-linker could also be used to control the reduction rate and in turn the core morphology. Both the optical spectra and the TEM images confirm that an increase in BIS content from 5% up to 17.5% (and consequently a decrease in shell pore size) slowed down the rate of gold reduction, yielding particles with a lower degree of branching (Fig. 5).

2.4. Optical Properties

In Au@pNIPAM colloids, the temperature-driven volume changes of the pNIPAM shell have been shown to affect the surface-plasmon resonance condition of the core metal nanoparticles, because of the associated changes in the local refractive index.[19,32] All of the nanocomposite systems studied in this work did indeed display a reversible shift in plasmon frequency during heating or cooling. Interestingly, the magnitude of the shift could be tuned through three different factors, namely, the percentage of cross-linker, the pNIPAM shell thickness, and the gold core size/shape. The effect of the cross-linking density on the optical response of the gold cores was studied by UV–vis spectroscopy. Figure 6A shows the influence of temperature on the UV–vis spectrum of the colloid for two core–shell systems with a 5% content of BIS. The profile of the temperature-induced band shift (Figure 6B) is similar to that observed by light-scattering or turbidity measurements following the absorbance at 400 nm (data not shown). At low temperature (shell is in the swollen state) no change is observed, but as the temperature increases the collapse of the shell produces a gradual shift of the plasmon band, and once the shell is fully collapsed it remains constant even if the temperature is raised further. As the cross-linker density decreases, the total shift increases from 7 nm to 11 nm, that is, the sensitivity of the surface-plasmon band decreases as the pNIPAM shell is more cross-linked. This trend can be explained considering the changes in the pNIPAM shell volume for the different samples considering that the particle size in the collapsed state is similar in all cases. Considering that the red-shift in the plasmon band is related to an increase in the local refractive index surrounding the particle as water is released from the pNIPAM shell, the maximum shift of the surface-plasmon band will be proportional to the shrinking ratio, which follows the trend: 9.66, 7.76, and 5.83 for 5, 10, and 17.5% BIS, respectively (from PCS analysis, see Table S1, Supporting Information).

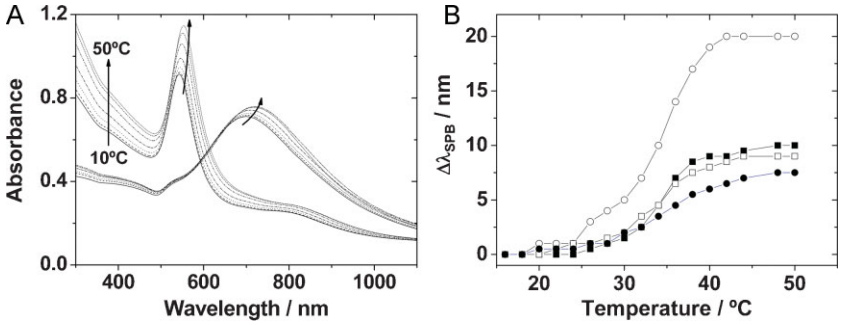

Figure 6. A) UV–Vis spectra at different temperatures, between 10 °C and 50 °C, of aqueous dispersions of spherical 59 nm (left) and branched (ca. 110 nm) (right) gold core@pNIPAM-shell nanoparticles with 5% BIS content. B) Surface-plasmon band shift with respect to the completely swollen state at 15 °C of different Au@pNIPAM composites: 59 nm gold core with a pNIPAM shell and different BIS content: (■) 5% BIS, (□) 10% BIS, (●) 17.5% BIS, and 110 nm branched core with a pNIPAM shell with 5% BIS (○).

Similarly, a variation of the pNIPAM shell thickness can determine the extent of the plasmon shift: a decrease in shell thickness from 185 nm to 95 nm in the fully swollen state (see Figure 3A) leads to a decrease in the SPB shift from 10 to 6 nm (data not shown). Additionally, the morphology of the gold core is another important factor to define the extent of the plasmon shift, since larger and more anisotropic gold particles are in general more sensitive toward refractive-index changes.[33] As an example, the collapse of the pNIPAM shell on 59 nm spheres and 120 nm branched gold cores leads to shifts of 10 nm and 20 nm, respectively (Figure 6).

3. Conclusions

pNIPAM-coated gold nanoparticles with a controllable degree of cross-linking and shell thickness were synthesized through varying the cross-linker density or the amount of monomers, or by adding small amounts of sodium dodecyl sulfate. Additionally, the cross-linker density influences the stiffness and porosity of the microgel, which was confirmed by PCS and AFM. It is interesting to stress that the size and shape of the gold cores could be tuned by controlling the diffusion rate of the reactants through the pNIPAM shell, either through the CTAB concentration or the porosity of the microgels. Since the shells retain the thermoresponsive properties of pure pNIPAM, the shell design can be used to modulate the optical properties of the gold cores. The unique properties of these shells allow us to control the seeded growth of the gold cores, with a fine shape design, which in turn nicely controls the resulting optical properties. Potential applications of this new class of nanocomposites are quite broad, ranging from quantitative analysis through direct SERS/surface-enhanced resonance Raman scattering (SERRS)/surface-enhanced fluorescence (SEF) sensing,[23] to photonic crystals, drug delivery,[34] and so on.

4. Experimental

Materials: Ascorbic acid (AA), cetyltrimethylammonium bromide (CTAB) sodium dodecyl sulfate (SDS), styrene, divinylbenzene (DVB) and *N*-isopropylacrylamide (NIPAM, 97%) were supplied by Aldrich. $HAuCl_4 \cdot 3H_2O$ and trisodium citrate dihydrate were supplied by Sigma. *N*,*N*′-methylenebisacrylamide (BIS) was supplied by Fluka. 2,2′-azobis(2-methylpropionamidine) dihydrochloride was supplied by Acros Organics. All reactants were used without further purification. Water was purified using a Milli-Q system (Millipore).

Synthesis of Au@pNIPAM Composites: In a typical synthesis, gold nanoparticles with a diameter of 59 ± 4 nm were prepared through a seeded growth method [29], based on the reduction of $HAuCl_4$ with ascorbic acid on CTAB-stabilized Au nanoparticle seeds (ca. 15 nm, previously prepared by citrate reduction), in the presence of 0.015 M CTAB. Subsequently, the particles were coated with polystyrene as follows: 150 mL of as-prepared CTAB-stabilized gold nanoparticles were centrifuged at 4500 rpm for 40 min, the supernatant was discarded, and the precipitate redispersed in 150 mL of milli-Q water. The solution was then heated to 30 °C, followed by addition of styrene (10 μL) and divinylbenzene (5 μL) under stirring. After 15 min the temperature was raised to 70 °C and the polymerization was initiated by adding 2,2′-azobis(2-methylpropionamidine) dihydrochloride (20 μL 0.1 M in water). The polymerization was allowed to proceed for 2 h. The solution was centrifuged at 4000 rpm (40 min), the supernatant discarded, and the precipitate redispersed in 15 mL of milli-Q water. The solution was purged with nitrogen (15 min), followed by addition of *N*-isopropylacrylamide (0.1698 g, 1.503 mmol, 100%, referred to as the standard amount) and *N*,*N*′-methylenebisacrylamide (0.0234 g, 0.150 mmol, 10% content with respect to NIPAM). After 15 min, the nitrogen flow was stopped and the polymerization was initiated by the addition of 2,2′-azobis(2-methylpropionamidine) dihydrochloride (150 μL, 0.1 M). After 7–10 min the reddish solution became turbid and the reaction was allowed to proceed for 3 h at 70 °C. The white mixture was then allowed to cool down to room temperature under stirring. To remove small oligomers, unreacted monomers, as well as gold free microgels, the dispersion was diluted with water (15 mL), centrifuged (30 min at 4000 rpm), and redispersed in water three times. The supernatants were discarded and the final precipitated was redispersed in water to obtain a Au@pNIPAM dispersion, 0.5 mM in terms of gold, that was then used as seeds for the core growth. The cross-linking density was varied by keeping constant the amount of NIPAM (0.1698 g, 1.503 mmol, 100%) and varying the amount of *N*,*N*′-methylenebisacrylamide (0.0117 g, 0.075 mmol, 5%; 0.0234 g, 0.150 mmol, 10%; and 0.0409 g, 0.263 mmol, 17.5%)

Controlling the pNIPAM Shell Thickness: The pNIPAM shell thickness was varied through two different approaches; a) changing the amount of NIPAM (0.1698 g, 1.503 mmol, 100%; 0.1273 g, 1.127 mmol, 75%; 0.0849 g, 0.7515 mmol, 50%; and 0.0679 g, 0.6012 mmol, 40%) and keeping the BIS content at 10 mol % with respect to that of NIPAM; and b) carrying out the standard synthesis as indicated above, in the presence of small amounts of sodium dodecyl sulfate (SDS), as indicated in the text.

Gold Core Overgrowth: The growth of the gold core was performed by seeded growth in aqueous CTAB. In a typical synthesis, 2.85 mL of growth solution was prepared containing 0.125 mM $HAuCl_4$ and CTAB (8 mM or 0.1 M to promote a spherical or branched morphology, respectively), followed by the addition of ascorbic acid to achieve the desired AA/$HAuCl_4$ ratio as indicated in the text. Finally, 0.15 mL of Au(59 nm)@pNIPAM seed solution (0.5 mM in terms of gold, see *Synthesis of Au@pNIPAM Composites*) were added.

Characterization: UV–Vis spectra were recorded using either a Cary 5000 UV-vis-NIR spectrophotometer or an Agilent 8453 UV-vis spectrophotometer. Atomic force microscopy was carried out in the tapping mode with a VEECO RTESP tip of $k = 20$–80 N m^{-1} (exact spring constant not calculated) using a Nanoscope V controller on a multimode microscope. Transmission electron microscopy was performed by using a JEOL JEM 1010 microscope operating at an acceleration voltage of 100 kV. Photon correlation spectroscopy (PCS) was carried out on a Zetasizer Nano S

(Malvern Instruments, Malvern UK) using a detection angle of 173°. The Nano S used a 4 mW He–Ne laser operating at a wavelength of 633 nm. The intensity-averaged particle diameter and the polydispersity index values (an estimate of the distribution width) were calculated from cumulative analysis. Raman spectra were measured on a LabRam HR (Horiba-Jobin Yvon) Raman system. PS/DVB characterization was performed under the microscope by centrifuging 15 mL of the corresponding suspension and casting the residue on a glass slide, Raman was recorded by exciting the sample with a 633 nm laser line (1 mW).

Acknowledgements

This work was supported by the Spanish Ministerio de Ciencia e Innovación, through Grants No. MAT2007-62696, MAT2009-14234-C03-02 and NAN2004-09133-C03-03, Xunta de Galicia (PGIDIT06TMT31402PR), and Junta de Andalucía through a scolarship (R. Contreras-Cáceres, project FQM-02353). In addition, partial support of COST Action D43 is acknowledged. The authors thank Dr. R. A. Álvarez-Puebla and C. Fernández-López for the Raman measurements and help with the synthesis, respectively. Supporting Information is available online from Wiley InterScience or from the author.

Received: March 20, 2009
Published online: August 19, 2009

[1] G. Kickelbick, L. M. Liz-Marzán, in *Encyclopedia of Nanoscience and Nanotechnology, Vol. 2*(Ed: H. S. Nalwa), American Scientific Publishers, Valencia, CA **2004**, pp. 199–220.
[2] J. Shan, H. Tenhu, *Chem. Comm.* **2007**, *44*, 4580.
[3] L. M. Liz-Marzan, M. Giersig, P. Mulvaney, *Langmuir* **1996**, *12*, 4329.
[4] Y. Deng, D. Qi, C. Deng, X. Zhang, D. Zhao, *J. Am. Chem. Soc.* **2008**, *130*, 28.
[5] T. Nann, P. Mulvaney, *Angew. Chem. Int. Ed.* **2004**, *43*, 5393.
[6] R. K. Iler, *The Chemistry of Silica*, John Wiley and Sons, New York, NJ **1979**.
[7] a) A. B. Lowe, B. S. Sumerlin, M. S. Donovan, C. L. McCormick, *J. Am. Chem. Soc.* **2002**, *124*, 11562. b) K. J. Watson, J. Zhu, S. T. Nguyen, C. A. Mirkin, *J. Am. Chem. Soc.* **1999**, *121*, 462.
[8] W. P. Wuelfing, S. M. Gross, D. T. Miles, R. W. Murray, *J. Am. Chem. Soc.* **1998**, *120*, 12696.
[9] a) M.-Q. Zhu, L.-Q. Wang, G. J. Exarhos, A. D. Q. Li, *J. Am. Chem. Soc.* **2004**, *126*, 2656. b) M. K. Corbierre, N. S. Cameron, R. B. Langmuir. Lennox, **2004**, *20*, 2867.
[10] G. Schneider, G. Decher, *Nano Lett.* **2004**, *4*, 1833.
[11] D. Gittins, F. Caruso, *J. Phys. Chem. B* **2001**, *105*, 6846.
[12] H. Dong, M. Zhu, J. A. Yoon, H. Gao, R. Jin, K. Matyjaszewski, *J. Am. Chem. Soc.* **2008**, *130*, 12852.
[13] P. J. Roth, P. Theato, *Chem. Mater.* **2008**, *20*, 1614.
[14] C. A. Mirkin, R. L. Letsinger, R. C. Mucic, J. J. Storhoff, *Nature* **1996**, *382*, 607.
[15] E. R. Zubarev, J. Xu, A. Sayyad, J. D. Gibson, *J. Am. Chem. Soc.* **2006**, *128*, 4958.
[16] J. P. Spatz, A. Roescher, M. Möller, *Adv. Mater.* **1996**, *8*, 337.
[17] S. Abraham, I. Kim, C. A. Batt, *Angew. Chem. Int. Ed.* **2007**, *46*, 5720.
[18] Y. Kang, T. A. Taton, *Angew. Chem. Int. Ed.* **2005**, *44*, 409.
[19] R. Contreras-Cáceres, A. Sánchez-Iglesias, M. Karg, I. Pastoriza-Santos, J. Pérez-Juste, J. Pacifico, T. Hellweg, A. Fernández-Barbero, L. M. Liz-Marzán, *Adv. Mater.* **2008**, *20*, 1666.
[20] M. Karg, I. Pastoriza-Santos, L. M. Liz-Marzán, T. Hellweg, *ChemPhysChem* **2006**, *7*, 2298.
[21] I. Gorelikov, L. M. Field, E. Kumacheva, *J. Am. Chem. Soc.* **2004**, *126*, 15938.
[22] S. Nayak, L. A. Lyon, *Angew. Chem. Int. Ed.* **2005**, *44*, 7686.
[23] R. Álvarez-Puebla, R. Contreras-Cáceres, I. Pastoriza-Santos, J. Pérez-Juste, L. M. Liz-Marzán, *Angew. Chem. Int. Ed.* **2009**, *48*, 138.
[24] A. M. Alkilany, R. L. Frey, J. L. Ferry, C. J. Murphy, *Langmuir* **2008**, *24*, 10235.
[25] R. Pelton, *Adv. Colloid Interface Sci.* **2000**, *85*, 1.
[26] W. McPhee, K. C. Tam, R. Pelton, *J. Colloid Interface Sci.* **1993**, *156*, 24.
[27] B. Sierra-Martín, A. Fernández-Nieves, M. S. Romero-Cano, A. Fernández-Barbero, *Langmuir* **2006**, *22*, 3586.
[28] B. Sierra-Martín, Y. Choi, M. S. Romero-Cano, T. Cosgrove, B. Vincent, A. Fernández-Barbero, *Macromolecules* **2005**, *38*, 10782.
[29] J. Rodríguez-Fernández, J. Pérez-Juste, F. J. García de Abajo, L. M. Liz-Marzán, *Langmuir* **2006**, *22*, 7007.
[30] J. Rodríguez-Fernández, J. Pérez-Juste, P. Mulvaney, L. M. Liz-Marzán, *J. Phys. Chem. B* **2005**, *109*, 14257.
[31] P. S. Kumar, I. Pastoriza-Santos, F. J. García de Abajo, L. M. Liz-Marzán, *Nanotechnology* **2008**, *19*, 015606.
[32] M. Karg, I. Pastoriza-Santos, J. Pérez-Juste, T. Hellweg, L. M. Liz-Marzán, *Small* **2007**, *3*, 1222.
[33] J. Rodríguez-Fernández, I. Pastoriza-Santos, J. Pérez-Juste, F. J. García de Abajo, L. M. Liz-Marzán, *J. Phys. Chem. C* **2007**, *111*, 13361.
[34] Y. Hu, T. Litwin, A. R. Nagaraja, B. Kwong, J. Katz, N. Watson, D. J. Irvine, *Nano Lett.* **2007**, *7*, 3056.